

Numerical Simulation of Collisionless Driven Reconnection Controlled by Multi-Scale Physics in Open Systems

Ritoku HORIUCHI^{1,2)}, Shunsuke USAMI¹⁾, Hiroaki OHTANI^{1,2)} and Mitsue DEN¹⁾

¹⁾*National Institute for Fusion Science, Toki 509-5292, Japan*

²⁾*The Graduate University for Advanced Studies, Toki 509-5292, Japan*

(Received: 28 August 2008 / Accepted: 17 November 2008)

Dynamical process of magnetic reconnection controlled by multi-scale physics is investigated using a series of numerical simulation models developed for the analysis of magnetic reconnection in open systems. Two dissipation regions with different spatial scales are formed inside the kinetic regime and a new force balance state is realized there through the combined action of the Hall effect and the effect of external driving source. MHD-PIC interlocked simulation scheme is developed based on domain decomposition method for the investigation of multi-scale physics in magnetic reconnection. The scheme is applied to propagation of MHD waves and is confirmed to work well.

Keywords: multi-scale simulation, magnetic reconnection, open systems, MHD model, PIC model

1. Introduction

Magnetic reconnection is widely believed to be one of important mechanisms controlling energetically active phenomena observed in high temperature, magnetized plasmas such as the solar flare, the magnetosphere, and laboratory experiments [1]. In spite of a long history of magnetic reconnection study there remain many problems unsolved. This is partly due to the fact that magnetic reconnection is controlled by multi-scale physics from microscopic electron dynamics to plasma transport in a macroscopic scale, which are mutually interacting with each other in complex ways. A microscopic process leading to the generation of electric resistivity such as wave-particle interaction [2, 3, 4, 5, 6] and binary collisions is needed to excite magnetic reconnection. On the other hand, global plasma transport and global change of field topology take place as a result of magnetic reconnection, which, in turn, affect reconnection mechanism itself through complex nonlinear processes. If there is an externally driving source or plasma inflow into the reconnection region, dynamical behavior of magnetic reconnection is largely affected by the external source. For example, an intermittent reconnection is observed to occur in the system with a constant energy supply from an external region [7, 8]. Thus, magnetic reconnection is a multi-scale phenomenon bridging between macroscopic and microscopic hierarchies, and its whole picture should be clarified by solving both microscopic physics and macroscopic physics consistently and simultaneously.

As a first step towards multi-scale simulation of magnetic reconnection, we have developed PArticle Simulation code for Magnetic reconnection in an Open system (PASMO) [8, 9, 10], which is subject to an external driving source. In this code the information of macroscopic system can be introduced into microscopic system as boundary conditions. Recently, MHD-PIC interlocked scheme for

the multi-scale simulation of magnetic reconnection has been developed based on domain decomposition method [11, 12]. This model consists of three parts, i.e., MHD model to describe global dynamics of reconnection phenomena, electromagnetic PIC model to describe the microscopic processes in the vicinity of reconnection point (i.e., PASMO code) and interface model to describe the interaction between micro and macro hierarchies. In this paper we discuss the microscopic physics of collisionless driven reconnection clarified by using PASMO code and give an overview of recent improvement of MHD-PIC interlocked scheme.

2. Open Boundary Model for PIC Simulation

Based on standard explicit electromagnetic PIC algorithm [13], we have developed the PASMO code with an open boundary model. In this model, a free condition is used at the downstream boundary ($x = \pm x_b$) and an input condition is used at the upstream boundary ($y = \pm y_b$) [8, 9, 10, 14]. The boundary condition for the z-axis is assumed to be periodic in three-dimensional case. The plasma inflows are symmetrically driven from two upstream boundaries by the external electric field imposed in the z direction under the assumption that the frozen-in condition is satisfied both for ions and for electrons. The driving field $E_{zd}(x, t)$ used for this simulation is the same as that in the previous simulations [8, 9, 10, 14], which is controlled by two parameters, i.e., maximum flux input rate E_0 and the spatial size of initial bell-shaped profile x_d (input window size).

Field quantities E_x , E_y and $\partial E_z / \partial x$ are assumed to be continuous at the downstream boundary ($x = \pm x_b$). The condition $\partial E_z / \partial x = \text{finite}$ allows the change in the y-component of magnetic field which is the necessary condition for a magnetic island to go freely through the boundary. Magnetic field at the boundaries is directly given by solving Maxwell equations there. The downstream bound-

author's e-mail: horiuchi.ritoku@nifs.ac.jp

ary condition for particles is determined under the assumptions that charge neutrality is maintained and the distribution functions are the same as those at one-grid inside position.

As an initial condition we adopt a one-dimensional equilibrium with the Harris-type configuration with anti-parallel magnetic field along x-axis as

$$B_x(y) = B_0 \tanh(y/L), \quad (1)$$

where B_0 is a constant and L is the scale height along the y-axis. There is a magnetically neutral sheet at $y = 0$ in the initial equilibrium. The initial particle distribution is assumed to be a shifted Maxwellian with spatially constant temperature and average particle velocity equal to the diamagnetic drift velocity.

The important parameters used for a three-dimensional simulation are as follows; the total number of particles is about 560 000 000, and the simulation domain is implemented on a $(256 \times 129 \times 128)$ point grid, the ratio of ion to electron temperature is $T_i/T_e = 1$, the ion Larmor radius associated with a magnetic field outside the current layer is $\rho_i = 0.93L$, and the ratio of the electron drift velocity to the electron thermal velocity is $v_{ze}/v_{te} = 0.21$, $m_i/m_e = 50$, and $\omega_{pe}/\omega_{ce} = 2.5$. The physical quantities used in this simulation are normalized by the light velocity c for velocity, c/ω_{ce} for spatial scale, and $1/\omega_{ce}$ for time.

3. Microscopic Physics of Collisionless Driven Reconnection

A series of numerical simulations using PASMO code have disclosed important microscopic pictures of collisionless reconnection [4, 8, 9, 10, 11, 14, 15]. In this section we describe new physical aspects of collisionless driven reconnection disclosed from recent numerical simulations. Temporal evolutions of reconnection electric field, electron number density per cell at the mid-point, and total number of particles are plotted in Fig. 1. After an initial transit phase ($\omega_{ce}t > 600$), the system relaxes to a steady state in which the inflow rate of magnetic flux ($E_0 = -0.04$) from the upstream boundary is balanced with the reconnection rate at the center ($E_z(0, 0, 0)$). Although total number of particle in the system, N_{pt} , is a function of time, its value is almost constant in the steady state, in the same way of the local physical quantities at the mid-point such as the number density $n_{e,mid}$.

Figure 2 demonstrates the spatial profiles of electron number flux (top) and out-of-plane magnetic field B_z (bottom) in the steady state ($\omega_{ce}t = 842$). The electron outflow with high velocity comparable to electron Alfvén velocity is generated from electron dissipation region, in which electron frozen-in condition is broken, as a result of collisionless reconnection, [15]. When the electron outflow reaches the downstream boundary, strong electron inflow should be supplied into the system to keep the charge neutrality, because the ion outflow velocity is usually much

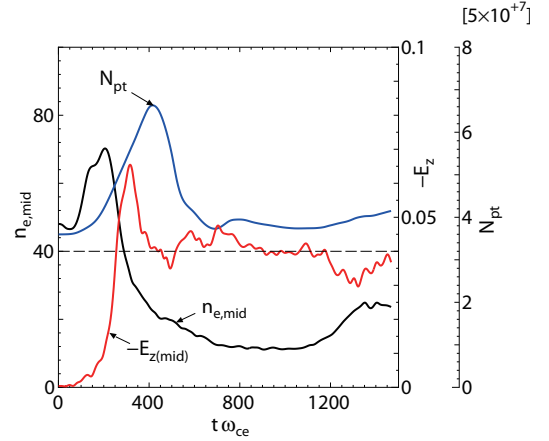


Fig. 1 Temporal evolutions of reconnection electric field (red), electron number density per cell at the mid-point (black), and total number of particles (blue).

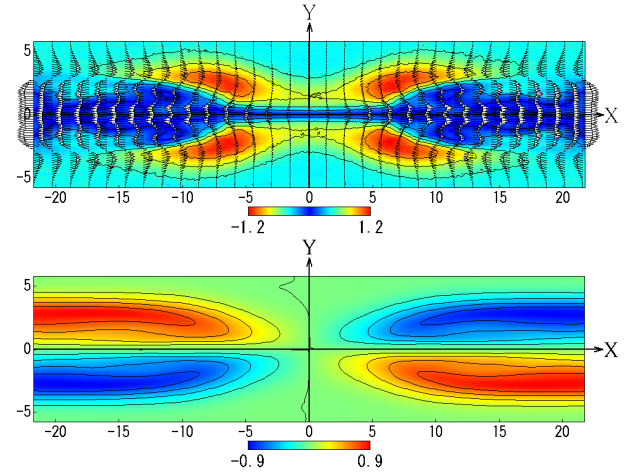


Fig. 2 Spatial profiles of electron number flux (top) and out-of-plane magnetic field B_z (bottom) in the (x,y) plane at $\omega_{ce}t = 842$, where color coded contours in the top panel stand for the number flux along the inflow (y) direction. In top panel, the red color represents the region in which the high inflow flux towards the center ($y=0$) exists.

smaller than the electron one in the kinetic regime and so the ions cannot compensate for the loss of electron charge at the downstream boundary. In other words, the balance of electron mass flux is quite different from that of magnetic flux (see Fig. 1). In this way, electron return current is formed along magnetic separatrix from the downstream boundary to the electron dissipation region. It is worthy to note that this physical process can be described only under

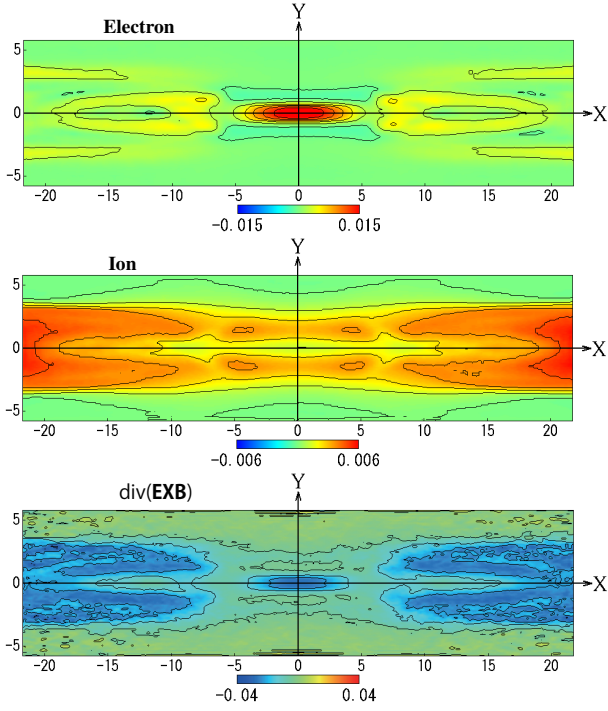


Fig. 3 Spatial profiles of normalized conversion rates of magnetic energy into electrons ($\mathbf{E} \cdot \mathbf{J}_e$)/ n_e (top) and ions ($\mathbf{E} \cdot \mathbf{J}_i$)/ n_i (middle), and the divergence of Poynting flux $\text{div}(\mathbf{E} \times \mathbf{B})$ (bottom) in the (x,y) plane at $\omega_{ce}t = 842$.

the open boundary model. Furthermore, this result is in contrast with that of classical Sweet-Parker model [16] in which uniform plasma inflow from the upstream boundary is assumed to be balanced with the plasma mass outflow from the dissipation region. The difference between the ion and electron motions in the reconnection plane leads to the generation of out-of-plane magnetic field B_z with quadrupole structure, as seen in the bottom panel of Fig. 2.

One of important features of magnetic reconnection is that magnetic energy can be effectively converted to plasma kinetic energy and/or thermal energy in a short time scale. Figure 3 illustrates the spatial profiles of normalized energy conversion rates to electrons ($\mathbf{E} \cdot \mathbf{J}_e$)/ n_e (top) and ions ($\mathbf{E} \cdot \mathbf{J}_i$)/ n_i (middle), and the divergence of Poynting flux $\text{div}(\mathbf{E} \times \mathbf{B})$ (bottom) in the (x,y) plane at $\omega_{ce}t = 842$, where the profiles are plotted after being averaged along the z direction. There are two specific regions where magnetic energy is effectively converted to plasma energies. Electrons get their energy through acceleration by the reconnection electric field in the central narrow region of the current sheet, while ions get their energy mainly in the vicinity of magnetic separatrix and the downstream. Thus, kinetic regime consists of two dissipation regions with different spatial scales, i.e., wide ion dissipation region (IDR) and narrow electron dissipation region (EDR) [9, 14, 17].

Frozen-in condition is broken due to kinetic processes in the dissipation regions. The violation mechanism of ion

and electron frozen-in conditions has been examined using the force balance equations in the out-of-plane direction in the previous studies [9, 14, 18] and it is found that, in the steady state, the main cause comes from the pressure tensor term which stands for the effect of non-gyrotropic motion in the vicinity of neutral sheet (meandering motion). Here, let us consider the force balance in the inflow direction. Figure 4 shows the spatial profile of forces acting on electrons (top) and those on ions in the inflow direction (y -direction) at $\omega_{ce}t = 842$ where the normalized charge density is also plotted along the y -axis in the top panel. Because ion becomes unmagnetized inside the IDR while electron remains still magnetized there, driving electric field works strongly on magnetized electrons to move inwards and electron-rich region is formed inside the EDR. Charge density changes its sign at the electron skin depth (see black dashed curve in the top panel of Fig. 4). Strong electrostatic field (red curve) is generated as a result of the charge separation in the kinetic regime and its value becomes maximum at the electron skin depth. The in-plane electrostatic force becomes dominant over the in-plane pressure force and inertia force terms around the electron skin depth, as shown in Fig. 4. Thus, initial Harris equilibrium is largely modified due to the existence of an external driving source and the Hall effects, and new force balance states are realized in EDR and IDR, respectively. Ion pressure gradient (blue curve) balances with the $\mathbf{J}_i \times \mathbf{B}$ force (black curve) in IDR, i.e.,

$$\frac{dp}{dy} = J_{iz} B_x. \quad (2)$$

Unmagnetized ions are accelerated inward directly by the electrostatic field as they approach the electron skin depth, and get the kinetic energy. On the other hand, the electron in-plane pressure force and inertia force terms are negligibly small inside EDR. Thus, the electrostatic force balances with the $\mathbf{J}_e \times \mathbf{B}$ force (black curve) in the inflow direction as

$$n_e e E_y = J_{ez} B_x \quad (3)$$

inside EDR. Because $J_{ez} \gg J_{iz}$ in EDR, Eq. 3 indicates that the electrostatic field balances with the Hall electric field $\mathbf{J} \times \mathbf{B}/n_e e$.

4. MHD-PIC Interlocked Scheme

Most of magnetic reconnection systems are open to external sources. Microscopic reconnection mechanism and its dynamical behavior in an open system are observed to be strongly dependent on the conditions of external driving source such as the flux inflow rate and its spatial profile [8, 9, 10]. In order to investigate the whole picture of magnetic reconnection we have developed MHD-PIC interlocked model based on the domain decomposition method [12]. That is, microscopic system, which is in charge of microscopic kinetic dynamics of magnetic reconnection in the vicinity of reconnection point and described

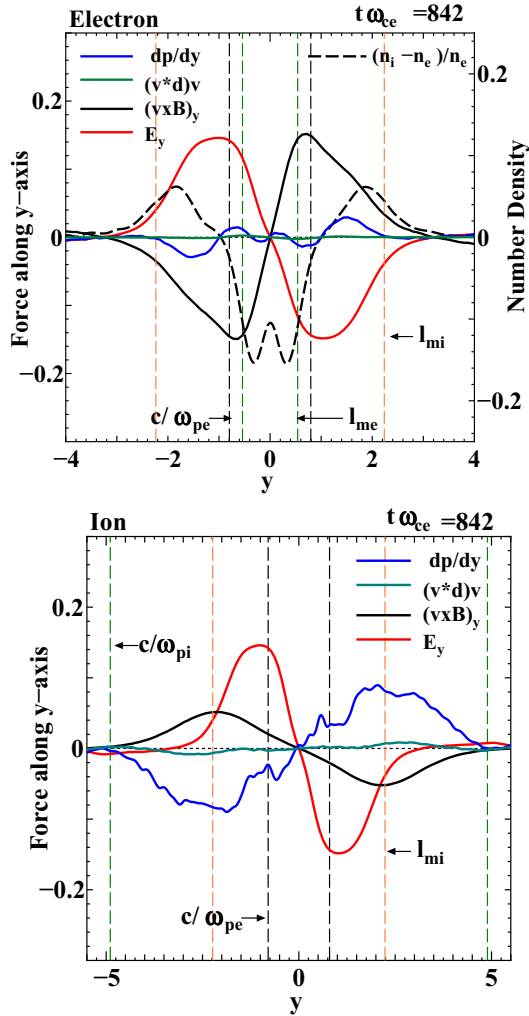


Fig. 4 Spatial profiles of forces acting on electrons (top) and those on ions in the inflow direction at $\omega_{ce}t = 842$ where the normalized charge density is also plotted along the y -axis in the top panel, and these profiles are plotted after being averaged over z -axis. Blue, green, black, and red curves stand for the pressure force, inertia force, Lorentz force, and electric force normalized by the local charge density, respectively. Black, orange, green dashed vertical lines stand for the locations at which the distances from the center are equal to electron skin depth, ion meandering scale, and electron meandering scale in the top panel, and equal to electron skin depth, ion meandering scale, and ion skin depth in the bottom panel, respectively.

by the PIC code (PASMO code), is connected with macroscopic system, which is responsible for the global dynamics far from the reconnection point and described by MHD code [20], through an interface domain. Both multi-time scale scheme [12] and shake-hand scheme [21] are also adopted for this interlocked model. We have performed numerical simulation of propagation of one-dimensional linear Alfvén wave in the simplified geometry to examine our interlocked model.

In the interface domain both the PIC and MHD sim-

ulations are performed and the physical quantities are defined as the interpolation value of the obtained quantities as

$$Q = \alpha(y)Q_{\text{MHD}} + (1 - \alpha(y))Q_{\text{PIC}}, \quad (4)$$

where the interpolation function $\alpha(y)$ changes from 0 to 1 according to the spatial position y , Q_{MHD} and Q_{PIC} are the field quantities obtained from the MHD and PIC simulations, respectively. Recently, we improved the interpolation scheme in order to satisfy the divergence-free condition of magnetic field exactly and the condition $d\alpha(y)/dy = 0$ at the boundary of the interface domain. The latter condition ensures that the field quantities can be smoothly connected with the MHD or PIC quantities at the boundary of the interface domain. That is, magnetic field in the interface domain is obtained from the rotation of the interpolated vector potential, and the interpolation function $\alpha(y)$ is assumed to have the form as

$$\alpha(y) = \frac{\cos(\phi(y)) + 1}{2}, \quad (5)$$

where

$$\phi(y) = \pi \frac{y - y_{\text{MHD}}}{y_{\text{PIC}} - y_{\text{MHD}}},$$

y_{PIC} and y_{MHD} are boundary positions of the interface domain on the PIC and MHD sides, respectively. Figure 5 demonstrates the propagation of one-dimensional Alfvén wave carried out as a numerical test of this interlocked scheme where a uniform external magnetic field exists in the y direction ($\mathbf{B} = (0, B_{y0}, 0)$), the electron thermal velocity is $v_{te} = 0.1c$, the wave amplitude is $B_x = 0.1B_{y0}$, $m_i/m_e = 100$, and $\omega_{pe}/\omega_{ce} = 1.0$. PIC domain is located in the center of the simulation box ($96 < y < 160$), and MHD domains are in both sides of PIC domain ($0 < y < 64$, $192 < y < 256$). There exists the interface domain between MHD and PIC domains ($64 < y < 96$, $160 < y < 192$). The periodic condition is adopted at the boundaries of the simulation domain. It is clearly seen in Fig. 5 that Alfvén wave is propagating from MHD domain to PIC domain, and from PIC domain to MHD domain smoothly except for small fluctuations in the PIC region. In other words, the present interlocked scheme works well.

5. Summary

We have investigated dynamical process of magnetic reconnection controlled by multi-scale physics based on a series of numerical simulation models developed for the analysis of magnetic reconnection in open systems. Electromagnetic PIC simulations using PASMO code with an open boundary model have disclosed that two dissipation regions with different spatial scales are formed inside the kinetic regime and a new force balance state is realized there through the combined action of the Hall effect and the effect of external driving source. MHD-PIC interlocked

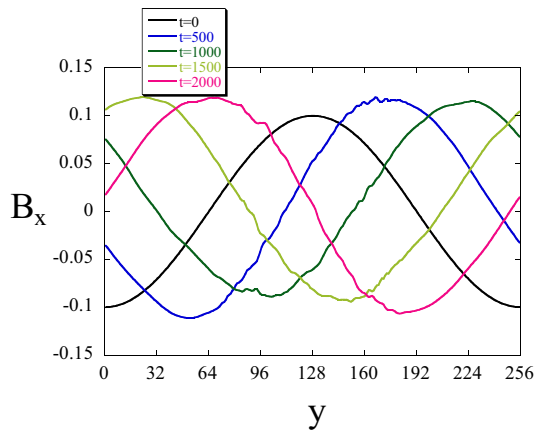


Fig. 5 Spatial profiles of magnetic field B_x at $\omega_{ce}t = 0, 500, 1000, 1500,$ and 2000 . Wave propagates in the right direction.

simulation scheme has been also developed based on domain decomposition method for the investigation of multi-scale physics in magnetic reconnection. This scheme consists of three parts, i.e., MHD model to describe global dynamics of reconnection phenomena, PIC model to describe the microscopic processes in the vicinity of reconnection point, and interface model to describe the interaction between micro and macro hierarchies. The developed scheme has been applied to propagation of MHD waves and confirmed to work well.

This work was partially supported by a Grant-in-Aid for Scientific Research from Japan Society for the Promotion of Science (No. 18340188), the Research Cooperation Program on "Hierarchy and Holism in Natural Sciences 2" at National Institutes of Natural Sciences, and General Coordinated Research at National Institute for Fusion Science (NIFS08KTAN005, NIFS08KTAL015).

[1] M. Yamada, *Phys. Plasma*, **14** (2007), 058102-1-16.
 [2] N. A. Krall and P. C. Liewer, *Phys. Rev.* **4**, 2094(1971).
 [3] Z. Zhu and R. M. Winglee, *J. Geophys. Res.* **101**, 4885(1996).
 [4] R. Horiuchi and T. Sato, *Phys. Plasmas* **6** 4565-4574 (1999).
 [5] W. Daughton, *Phys. Plasmas* **6**, (1999), 1329.
 [6] T. Moritaka, R. Horiuchi, and H. Ohtani. *Phys. Plasmas* **14**, (2007), 102109.
 [7] H. Amo, T. Sato, A. Kageyama, K. Watanabe, R. Horiuchi, T. Hayashi, Y. Todo, T. H. Watanabe, and H. Takamaru, *Physical Review* **E51** 3838-3841 (1995).
 [8] W. Pei, R. Horiuchi and T. Sato, *Phys. Plasmas* **8** 3251-3257 (2001).
 [9] W. Pei, R. Horiuchi and T. Sato, *Phys. Rev. Lett.* **87** 235003-1-235003-4 (2001).
 [10] R. Horiuchi, H. Ohtani, and A. Ishizawa, *Comp. Phys. Comm.* **164**, 17-22 (2004).
 [11] R. Horiuchi, H. Ohtani, and A. Ishizawa, *J. Plasma Phys.* **72** 953-956 (2006).
 [12] S. Usami, H. Ohtani, and R. Horiuchi, *Comm. Comp. Phys.* **4** 537-544 (2008).
 [13] C. K. Birdsall and A. B. Langdon, *Plasma Physics via Computer Simulation* (McGraw-Hill, New York, 1985).

[14] A. Ishizawa and R. Horiuchi, *Phys. Rev. Lett.* **95** 045003-1-045003-4 (2005).
 [15] R. Horiuchi and H. Ohtani, *Comm. Comp. Phys.* **4** 496-505 (2008).
 [16] D. Biskamp, *Magnetic Reconnection in Plasmas* (Cambridge University Press, Cambridge, 2000)
 [17] M. A. Shay, J. F. Drake, B. N. Rogers, and R. E. Denton, *J. Geophys. Res.* **106**, 3759 (2001).
 [18] M. Hesse, K. Schindler, J. Birn, and M. Kuznetsova, *Phys. Plasmas* **6** (1999),1781 .
 [19] W. Daughton, J. Schdder, and H. Karimabadi, *Phys. Plasmas* **13**, (2006), 072101.
 [20] R. Horiuchi and T. Sato, *Phys. Fluids*, B1 (1989) 581.
 [21] T. Sugiyama and K. Kusano, *J. Comput. Phys.*, **227** (2007) 1340.